A99-16306

AIAA 99-0413

DNS Evaluation of Chemistry Models for Compressible Non-Premixed Flames

Foluso Ladeinde, Wei Liu, & Edward E. O'Brien
State University of New York, Stony Brook
Department of Mechanical Engineering
Stony Brook, L.I., New York 11794-2300

37th AIAA Aerospace Sciences Meeting and Exhibit
January 11-14, 1999 / Reno, NV

DNS EVALUATION OF CHEMISTRY MODELS FOR TURBULENT, REACTING, AND COMPRESSIBLE MIXING LAYERS

Foluso Ladeinde*, Wei Liu+, & Edward E. O'Brien#
Mechanical Engineering Department
SUNY at Stony Brook
Stony Brook, L.I., New York

Abstract

In this paper, we use the direct numerical simulation (DNS) approach to carry out fundamental studies that compare the performance of an eight-step/seven-species chemistry model and a model consisting of twenty-five steps and twelve species. The basic H_2 - Air reaction is used, because of the relevance to combustion in turbomachinery and the scramjet engines, and results are presented for $M_c = 0.8$, where M_c is the convective Mach number. Various definitions of the layer growth rate are used in an attempt to differentiate compressibility effects of high-speed from those of chemical reaction. The standard vorticity thickness definition, which is biased toward the hydrodynamic part of the flow, shows a similar evolution for both chemistry models and the non-reacting case. However, three other definitions, which depend on the extent of chemical reaction, show considerably different temporal evolution for the two chemistry models. In general, the twenty-five step model shows more vigorous reaction. Also observed for the 25-step system is the extraction of energy from the system, which is manifested as lower-than-upstream temperatures away from the centerline of the layer. We attribute this to the endothermic nature of some of the reaction steps. Examination of the anisotropy tensor shows no effect of chemistry or its modeling. However, no particular attention was paid to the integral length scale, i.e., the normalized initial correlation between scalar values in adjacent nodal points of the grid.

1. Introduction

In comparison to detailed chemistry, reduced chemistry models have the advantage of computational efficiency and are therefore preferred in situations where they could produce acceptable results. Some chemistry models for H_2 - *Air* combustion in non-premixed situations have been investigated in our work, using direct numerical simulation (DNS), with the objective of determining the acceptability of the simpler, but affordable, models. The interest is in convective Mach numbers, M_c, in the range $0.2 \leq M_c \leq 3.0$, with Arrhenius-type relations for chemistry models which vary from the simple one-step/three-species type to the twenty-five step/twelve-species reactions. Each of the steps in these reactions possesses its own effective Damkholer number and the various species, in general, have different diffusivities (Schmidt numbers). These parameters were not varied in our simulation. Studies on high speed and non-premixed chemical reactions include Drummond[1] and the review article by Dimotakis[2]. However, these studies included neither direct numerical simulation nor the effect of different chemistry models. Givi et al.[3] used DNS to investigate compressibility and heat release effects in a high-speed mixing layer but considered only a single step reaction. Chakraborty et al.[4] calculated reacting mixing layers with multi-step chemistry models but only a 7-step, 8-species chemistry model was considered.

Evans and Schexnayder[5] studied the influence of the same chemical kinetics as in this paper and of unmixedness on burning in

* Associate Professor, Associate Fellow, AIAA
+ Research Assistant
# Professor

supersonic hydrogen flame. However, the Reynolds-averaged approach was used, with some turbulence and chemistry closure models. This differs from the rather fundamental approach in the present work, where DNS obviates the need for closure models.

2. Model Details

The mixing layer is considered here as a prototype of the scramjet engine, with a focus on compressible flows, turbulence and chemical reaction. Linear stability analysis for the non-reacting system shows that, for convective Mach numbers, M_c, greater than 0.6, the oblique shock wave modes of excitation have the growth rate advantage to dominate the flow and make the flow three-dimensional at the onset of instability. However, in this paper, we will beg this issue with confinement and heat release arguments, which tend to make reacting mixing layer flow two-dimensional (2D). Moreover, we are forced to use a 2D model by virtue of the resolution requirements for DNS and the shear number of partial differential equations for a multi-species reaction model. Comments supporting 2D models for reacting flows have been made by Higuera and Moser [6].

The DNS procedure in the present work is based on the ENO schemes, which we have demonstrated to be suitable for compressible turbulence (Ladeinde et al. [7,8]; Cai et al. [9,10]). The versions of our codes that run on parallel machines are particularly of interest (Ladeinde et al. [11] and Cai et al. [9,12]). The calculations were done on the parallel SP/2 system under the NSF-supported NPACI program at the San Diego Supercomputing Center (SDSC). We calculate instantaneous values of density, ρ, mass flux, ρu_i, pressure, p, total energy, E, and the species mass fractions, $\rho\phi_i$. We also calculate the terms in the evolution equations for the Reynolds stress tensor,
as well as those in the evolution equations for the probability density function description for the mass and mixture fraction. Although fuels such as N-heptane could easily be used in our code, we have chosen hydrogen. The oxidant is oxygen, with the overall reaction

$$2H_2 + O_2 \underset{k_b}{\overset{k_f}{\Leftrightarrow}} 2H_2O + \text{Heat}.$$

The Arrhenius approach is used to model the reaction rates for the steps and literature models are used.

The grid size for the numerical calculations is determined from the Kolmogorov scales, not the Batchelor scales. The numerical approach is used in the capturing implementation, although it is particularly suitable for resolving large gradients at flame fronts, compared to other competing methods. Most of the calculations are done on a 256^2 grid, with a few on 128^2 and 512^2.
The following eight-step/seven-species reversible reaction model was analyzed using DNS:

No.	Reaction
1	$H_2 + M \Leftrightarrow H + H + M$
2	$O_2 + M \Leftrightarrow O + O + M$
3	$H_2O + M \Leftrightarrow OH + H + M$
4	$OH + M \Leftrightarrow O + H + M$
5	$H_2O + O \Leftrightarrow OH + OH$
6	$H_2O + H \Leftrightarrow OH + H_2$
7	$O_2 + H \Leftrightarrow OH + O$
8	$H_2 + O \Leftrightarrow OH + H$

No.	A_f	B_f	C_f	A_b	B_b	C_b
1	5.5×10^{18}	-1.0	51987	1.8×10^{18}	-1.0	0
2	7.2×10^{18}	-1.0	59340	4.0×10^{17}	-1.0	0
3	5.2×10^{21}	-1.5	59386	4.4×10^{20}	-1.5	0
4	8.5×10^{18}	-1.0	50830	7.1×10^{18}	-1.0	0
5	5.8×10^{13}	0	9059	5.3×10^{12}	0	503
6	8.4×10^{13}	0	10116	2.0×10^{13}	0	2600
7	2.2×10^{14}	0	8455	1.5×10^{13}	0	0
8	7.5×10^{13}	0	5586	3.0×10^{13}	0	4429

The seven species are: H_2, H_2O, OH, H, O, and N_2 (inert). The Arrhenius reaction rates are:

$$k_i = A_i \bullet T^{B_i} \bullet \exp(-C_i / T)$$

where A_i, B_i and C_i are listed in the above table for forward (with subscript f) and backward (subscript b) reactions. Note that the units of the constants in the table are such that the reaction rate k is in [cm^3/g-mole-sec] or [cm^6/(g-mole)^2-sec]. The equations for the twenty-five step, twelve-species model are shown in the table below.

No.	Reactions
1	$HNO_2 + M \Leftrightarrow NO + OH + M$
2	$NO_2 + M \Leftrightarrow NO + O + M$
3	$H_2 + M \Leftrightarrow H + H + M$
4	$O_2 + M \Leftrightarrow O + O + M$
5	$H_20 + M \Leftrightarrow OH + H + M$
6	$OH + M \Leftrightarrow O + H + M$
7	$HO_2 + M \Leftrightarrow H + O_2 + M$
8	$H_2O + O \Leftrightarrow OH + OH$
9	$H_2O + H \Leftrightarrow OH + H_2$
10	$O_2 + H \Leftrightarrow OH + O$
11	$H_2 + O \Leftrightarrow OH + H$
12	$H_2 + O_2 \Leftrightarrow OH + OH$
13	$H_2 + O_2 \Leftrightarrow H + HO_2$
14	$OH + OH \Leftrightarrow H + HO_2$
15	$H_2O + O \Leftrightarrow H + HO_2$
16	$OH + O_2 \Leftrightarrow O + HO_2$
17	$H_2O + O_2 \Leftrightarrow OH + HO_2$
18	$H_2O + OH \Leftrightarrow H_2 + HO_2$
19	$O + N_2 \Leftrightarrow N + NO$
20	$H + NO \Leftrightarrow N + OH$
21	$O + NO \Leftrightarrow N + O_2$
22	$NO + OH \Leftrightarrow H + NO_2$
23	$NO + O_2 \Leftrightarrow O + NO_2$
24	$NO_2 + H_2 \Leftrightarrow H + HNO_2$
25	$NO_2 + OH \Leftrightarrow NO + HO_2$

The twelve species in this model are H, O, H_2O, OH, O_2, H_2, N_2, N, NO, NO_2, HO_2, and HNO_2. The constants in the 25-step reaction system are shown in a table at the end of this paper.

The conservation equations (mass, momentum, species, and total energy) can be written in the following non-dimensional forms:

$$\frac{\partial \rho}{\partial t} + \frac{\partial (\rho u_j)}{\partial x_j} = 0$$

$$\frac{\partial (\rho u_i)}{\partial t} + \frac{\partial (\rho u_i u_j + p\delta_{ij})}{\partial x_j} = \frac{1}{\mathrm{Re}} \frac{\partial \tau_{ij}}{\partial x_j}$$

$$\frac{\partial (\rho \phi_r)}{\partial t} + \frac{\partial (\rho u_i \phi_r)}{\partial x_i} = \frac{\partial}{\partial x_i}\left(\frac{1}{\mathrm{Re} \cdot Sc_r} \rho \frac{\partial \phi r_r}{\partial x_i} \right) + \rho \omega_r,$$

$$r = 1,2 \cdots, N,$$

$$\frac{\partial E}{\partial t} + \frac{\partial [(E+p)u_j]}{\partial x_j} = \sum_{r=1}^{N} \frac{\partial}{\partial x_i}\left(\frac{1}{\mathrm{Re} \cdot Sc_r} \rho h_r \frac{\partial \phi_r}{\partial x_i} \right)$$

$$+ \frac{1}{\mathrm{Re}} \frac{\partial (u_j \tau_{ij})}{\partial x_j} - \frac{\partial q_j}{\partial x_j} - \sum_{r=1}^{N} \rho h_{r0} \omega_r,$$

where

$$E = \frac{p}{\gamma - 1} + \frac{1}{2}(\rho u_i u_i),$$

$$\tau_{ij} = \mu\left(\frac{\partial u_i}{\partial x_j} + \frac{\partial u_j}{\partial x_i} - \frac{2}{3} \frac{\partial u_k}{\partial x_k} \delta_{ij} \right)$$

Above, ϕ_r is the r-th species mass fraction. The expression for ω_r can be obtained as fellows. The following equation can be written for a system involving N species and M reaction steps:

$$\sum_{r=1}^{N} \nu'_{rs} M_r \underset{k_b}{\overset{k_f}{\Leftrightarrow}} \sum_{r=1}^{N} \nu''_{rs} M_r, \qquad s = 1,2....,M.$$

where M_r is the chemical symbol for species r, ν'_{rs} and ν''_{rs} are the constant stoichiometric coefficients for species r appearing as reactant and product, respectively, in reaction s. For species r, the contributions of all reactions can be expressed as

$$\omega_r = \sum_{s=1}^{M} \omega_r^s.$$

Here, ω_r^s is the mass rate of production per unit volume for the r-th species by the s-th reaction step, written as (Williams[13]):

$$\omega_r^s = (\nu''_{rs} - \nu'_{rs}) k_{f_s} \rho^{m_s} \prod_{r=1}^{N} (\phi_r)^{\nu'_{rs}} \cdot \left(1 - \frac{k_{b_s}}{k_{f_s}} \rho^{n_s - m_s} \prod_{r=1}^{N} (\phi_r)^{\nu''_{rs} - \nu'_{rs}} \right),$$

where

$$m_s = \sum_{r=1}^{N} \nu'_{rs}, \quad n_s = \sum_{r=1}^{N} \nu''_{rs}$$

are the overall order of the forward and backward reactions, respectively.

Note that non-dimensionalization is done using reference length scale L, velocity components by reference velocity U, density by $\rho_{Ref.}$ time by L/U, energy, E and pressure, p, by $\rho_{Ref}U^2$, temperature by T_{Ref}, and enthalpy by U^2. E is the explicit internal energy, with the corresponding enthalpy $H = E + p/\rho$,

$$H = \int_{T_0}^{T} C_p(T)dT; Ce^{\alpha} = h_o^d / C_v T_\infty$$

where
s the heat release parameter, which is considered a constant for the different species in our calculation.

3. The Initial and Boundary Conditions

The temporal mixing layer approach is used in our study and is initialized by the hyperbolic tangent mean velocity profile with superposed perturbations. The parameter set in the equations is: Re = 400, Pr = 1.4, Ce = 1.5, Sc = 0.5. The reference variables are: U = 272 m/s (M_c = 0.8, c = 340 m/s), L = 0.001 m, T_{Ref} = 2000 K, ρ_{Ref} = 0.1765 kg/m^3 (density of air at T_{Ref}). The initial mean velocity profile in all cases is $\bar{u}$ = tanh (2y), where y is the traverse coordinate. The streamwise coordinate is denoted by x. The initial mean temperature profile is calculated using the Crocco-Buseman relation and, assuming unit Prandtl number:

$$\bar{T} = 1 + M_c^2 \frac{(\gamma - 1)}{2}\left(1 - \bar{u}^2\right)$$

where γ is the ratio of specific heats and M_c is the free-stream Mach number (or convective Mach number). Uniform, scaled, non-fluctuating pressure is assumed for the initial mean flow ($\bar{p}_0$ = 1) and the mean density profile is obtained from:

$$\bar{p}_0 = \frac{\bar{\rho}_0 \bar{T}_0}{\gamma M_c^2}.$$

The following initial velocity disturbances were superimposed on the hyperbolic tangent profile:

$$u' = A_m \frac{yL_x}{10\pi}\sin\left(\frac{2\pi x}{L_x}\right)e^{-\frac{y^2}{10}},$$

$$v' = A_m \cos\left(\frac{2\pi x}{L_x}\right)e^{-\frac{y^2}{10}},$$

where the amplitude A_m is chosen to be 0.05 and L_x is the length of the domain in the x-coordinate direction. Above, u' is the x-component (streamwise) of the fluctuating velocity, v' is the y-component (transverse). The computational domain is (x,y) in (0, 20) X (-50, 50). The v' perturbation above, which decays to zero at the free stream, has been chosen to resemble the most-unstable eigenfunction from the linear theory, while the u' perturbation is such that the entire disturbance is divergence-free initially. The initial conditions for the species are given by

$$\phi_{H_2} = 0.4(1 + \tanh(2y)), \phi_{O_2} = 0.8 - \phi_{H_2},$$
$$\phi_{N_2} = 0.2, \phi_{Others} = 0$$

so that the mass concentrations of all species will add up to 1 initially. For boundary condition, periodicity is assumed streamwise and zero gradient free-stream. This is the case for all primary dependent variables in the governing equations. Finally, no numerical "spark-plug" was implemented in these studies; the approaching streams seem to possess high enough temperature (2000K) for "spontaneous" reaction.

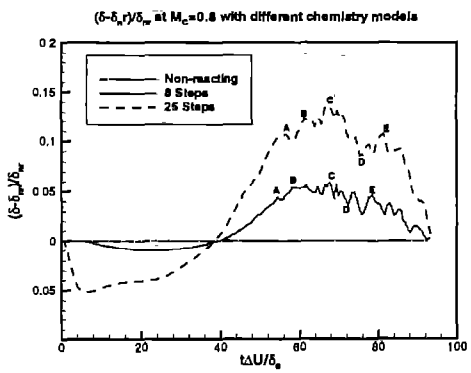

Fig.1: Evolution of the vorticity thickness.

4. Results and Discussion

The result shown in Figures 1 through 6 illustrate the effect of chemical reaction and of the chemistry model for M_c = 0.8. In Fig. 1, we show the layer growth rate for reacting and non-reacting flows, as a function of the eddy turn

over time, $t_e = t\Delta\mathcal{U}/\delta_o$, where t is the non-dimensional simulation time, $\Delta\mathcal{U}$ is velocity difference between the top and bottom streams, and δ_o is the initial vorticiy thickness. First, it is evident that chemical reaction affects the growth rate by as much as 6% (8 reactions) and 13% (25 reactions). We also observe that prior to $t_e \approx 40$, chemical reaction causes a reduction in the layer growth rate, as in some reports for incompressible flows. However, after this time, we observe a higher growth rate with chemistry, with the 25-reaction system showing the most activity. The intersection of the three curves in Figure 1 at $t_e \approx 40$ is evident. Because this is a temporal simulation, it could be argued that this point represents some type of stagnation. The coincidence is consistent with the fact that the downstream extent of the vortex structure is identical for the three cases, which isn't surprising because the convective Mach number is the same for the three cases. The figure also shows superposed oscillations over the profile for the non-reacting case. The oscillations appear correlated for the two reacting cases, as shown by the points A-B-C-D-E in the 8-reaction system and the corresponding points A'-B'-C'-D'-E' in the 25-reaction system. Obviously, the details of the oscillations are different for the two cases. The maximum amplitude of the oscillations relative to the local vorticity thickness of the non-reacting case is $\approx$ 2%, suggesting that the oscillations observed in Fig 1 may not be important.

Both high-speed and chemical reaction independently causes compressibility effects, so it is not a simple matter identifying the precise cause in a system as the present one where both factors are present. The classical vorticity thickness definition

$$\delta_\omega = \frac{\Delta U_\infty}{\left|\frac{d\bar{u}}{dy}\right|_{y=0}},$$

where the double overbar indicates averaged quantity, doesn't contain explicit chemical reaction dependence. We have defined three other types of layer thickness, which depend on reaction:

> δ_m $(x\ ;\ t)$: the farthest y-distance on the top stream where we find at most 1% of the bottom stream fluid (O_2) plus the farthest y-distance on the bottom stream where we find at most 1% of the top stream fluid (H_2),
>
> δ_p $(x\ ;\ t)$: the sum of the farthest y-distance on the top and bottom streams where we find at most 1% of the product (H_2O),
>
> δ_v $(x\ ;\ t)$: the farthest y-distance on the top stream where we find at least 99% of the top stream fluid (H_2) plus the farthest y-distance on the bottom stream where we find at least 99% of the bottom stream fluid (O_2).

Obviously in the foregoing, distances are measured from the center of the layer. δ_m, or mixing thickness, is actually a measure of mixing, or the extent to which the vortex structure has been able to bring the bottom fluid to the top layer and vice-versa. Obviously, δ_m need to be significant for reaction to occur to any significant level. δ_p, or the product thickness, is a measure of the spatial extent of reaction. δ_v, the visual thickness, is a measure of the layer thickness in the sense of species distribution.

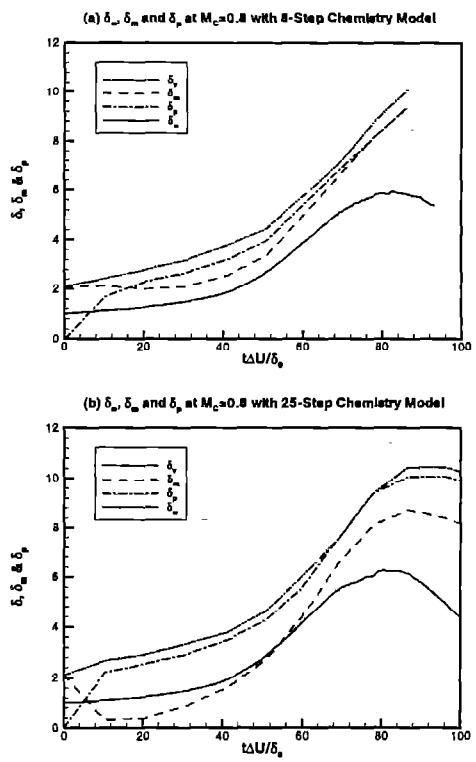

Fig. 2: Evolution of various thickness definitions: (a) 8-step, (b) 25-step.

Figures 2a and 2b are plots of the temporal evolution of the various layer thickness definitions (δ_ω, δ_m, δ_p, and δ_v), which show that

for either chemistry model, the layer definitions have different magnitudes. For the 8-reaction system profiles of the various thickness definition are quite similar with the major differences being in their relative magnitudes. As expected, δ_v has the largest magnitude and, because of the convection pattern, this is followed by δ_p and then by δ_m. Note that in the outer regions of the layer, but away from the free-streams, water formation is more likely than fluid from the opposite side of the layer, which would explain why $\delta_p \geq \delta_m$ after the initial transients. The lack of correlation between δ_w and the other vorticity definitions is quite evident for the 25-reaction system, where divergence in between the various definitions become pronounced for $t_e \geq 75$. For this chemistry model, the vorticity thickness is not an effective measure of the spatial extent of mixing or chemical reaction. We can only explain this in terms of the more vigorous reactions leading to the production of water. The relative reaction extent for the two chemistry models as, depicted in Fig 3a and 3b shows that the 25-reaction system is more vigorous than the 8-reaction system.

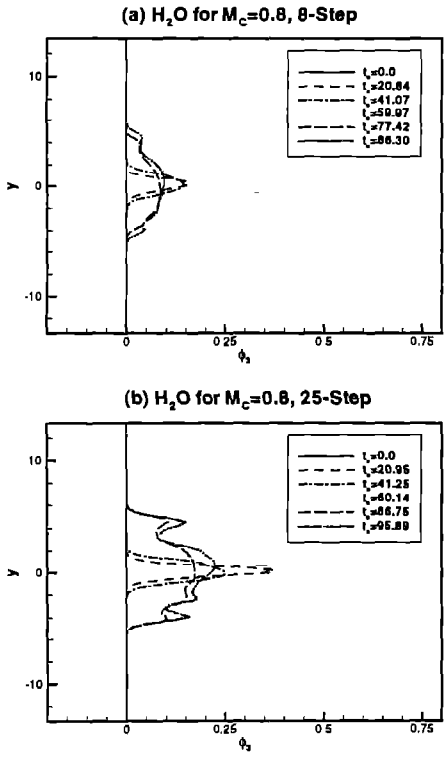

Fig. 3: Evolution of mass concentration of water: (a) 8-step, (b) 25-step.

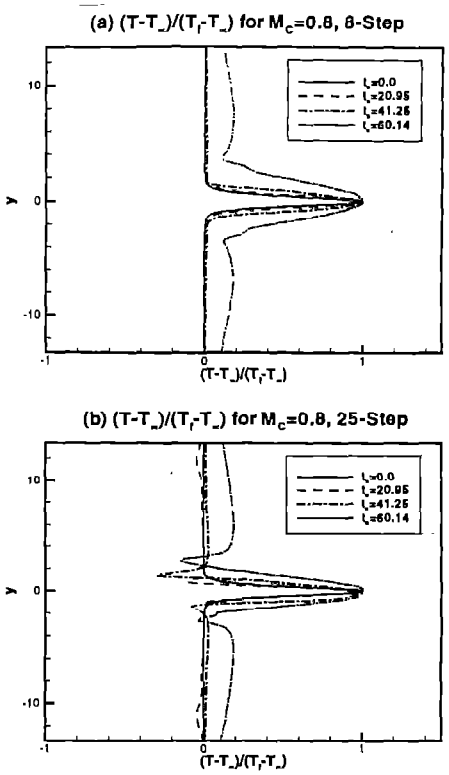

Fig. 4: Evolution of the heat release parameter θ: (a) 8-step, (b) 25-step.

To further isolate chemistry effects from high-speed compressibility, we investigated the normalized temperature profile.

$$\theta(y) = \frac{T(y) - T_\infty}{(T_{ad} - T_\infty)}$$

where T_∞ is the temperature of the unreacted mixtures and T_{ad} is the adiabatic flame temperature, for which we have used the maximum temperature, which occurs around $y = 0$. Early in the transient, the profile of $\theta(y)$ shows a similar development for the two chemistry models (Figure 4). However, for $t_e \geq 20$, we notice a strange development in the 25-reaction system, whereby energy is being drawn from the system, manifested in temperature values which are lower than the that in the unreacted streams. Our first reaction was to attribute the observation to numerical difficulties. However, a rigorous diagnosis didn't support a numerical artifact. So, we conclude that the phenomenon, which didn't show up in the 8-step reaction system, was probably a true reflection of the physics of the 25-reaction system. Some endothermic reaction steps are the likely cause of this phenomenon.

Finally, note that, whereas, the peak θ occurs at y = 0 for all time for the 8-reaction system, its position changes slightly with time for the 25-reaction system. The asymmetry in the θ profile for the 25-reaction system is also evident.

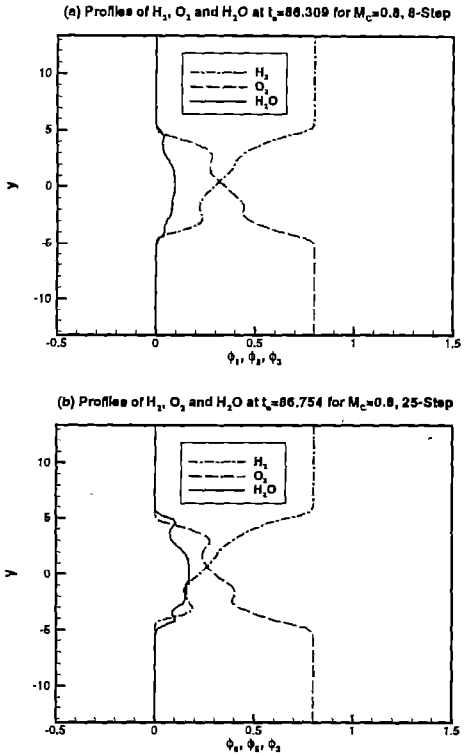

Fig. 5: Distribution of the primary reactants and product at $t_e \approx 86$: (a) 8-step, (b) 25-step.

Figures 5a and 5b show the y-dependence of the mass fraction of H_2, O_2, and H_2O at an eddy turnover time of approximately 86. We can observe in the 25-reaction system a larger region within $-5 \le y \le 6$ where the concentration of H_2O is actually greater than that of either O_2 or H_2. Figure 6 shows the short-time evolution of the anisotropy tensor:

$$B_{ij} = \overline{u_i'' u_j''} / 2K - (1/3)\delta_{ij};$$

where $K = (1/2)\ \overline{u_i'' u_i''}$; is the kinetic energy of turbulence. All components of B_{ij} are shown in the figure, as are the result for the non-reacting and the reacting cases. The conclusion is simple: chemical reaction doesn't affect the anisotropy tensor for the time range shown. However, the calculations in this paper were done without paying particular attention to the initial species integral length scale, i.e., the normalized initial correlation between species in neighboring nodal points. Recent studies seem to suggest that this might be important in some incompressible cases[14]. The situation with the compressible case is less certain, and no information in available yet on the species integral length scale for flows with shock waves.

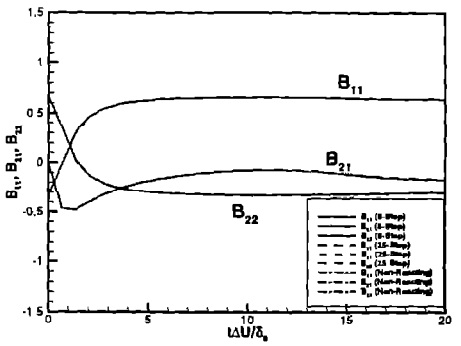

Fig. 6: Evolution of the anisotropy tensor.

Acknowledgements

The authors acknowledge NSF funding (CTS-9626413) for this study.

References

[1] Drummond, J.P., "A two-dimensional numerical simulation of supersonic chemically reacting mixing layer," NASA Technical Memorandum 4055, December 1988.

[2] Dimotakis, P. E., "Turbulent free shear layer mixing and combustion," In *High-Speed Flight Propulsion Systems*, Edit. S.N.B. Murthy & E.T. Curran, Vol. 137 of Progress in Aeronautics and Astronautics. Publ. American Institute o Aeronautics and Astronautics, Washington, D.C., 1991.

[3] Givi, P., Madnia, C.K., Steinberger, C.J., Carpenter, M.H., and Drummon, J.P., "Effects of Compressibility and Heat Release in a High Speed Reacting Layer," Combust. Sci. and Tech., Vol. 78, 1991, pp. 33-67.

[4] Chakraborty, D., Nagaraj Upadhyaya, H. V., Paul, P. J., and Mukunda, H. S., "A thermo-chemical exploration of a two-dimensional reacting supersonic mixing layer," Phys. Fluids, Vol. 9, 1997, pp. 3513-3522.

[5] Evans, J.S. and Schexnayder, C.J., "Influence of Chemical Kinetics and Unmixedness on Burning in Supersonic Hydrogen Flames," AIAA Journal, Vol. 18, No 2, 1980, pp. 188-193.

[6] Higuera, F.J. & Moser, R.D., "Effect of chemical heat release in a temporally evolving mixing layer," *Proc. 1994 Summer Program*, Center for Turbulence Research, NASA Ames/Stanford University, December 1994.

[7] Ladeinde, F., O'Brien, E. E., Cai, X., & Liu, W. "Advection by polytropic compressible turbulence," *The Phys. Fluids*, 48 (11), 1995, pp. 2848-2857.

[8] Ladeinde, F. Liu, W., & O'Brien, E. E., "Turblence in compressible mixing layers," *J. Fluids Engineering*, 120 (1), 1998, pp.48-53.

[9] Cai, X, O'Brien, E. E. & Ladeinde, F., "Uniform mean scalar gradient in grid turbulence: asymptotic probability distribution of a passive scalar," *The Phys. Fluids* 8(9), 1996, pp.2555-2558.

[10] Cai, X., O'Brien, E. E. & Ladeinde, F., "Thermodynamic behavior in decaying, compressible turbulence with initially dominant temperature fluctuations," *The Phys. Fluids* 9(6), 1997, pp. 1754-1763.

[11] Ladeinde., O'Brien, E.E. & Cai, X., "An Efficient Parallelized ENO Procedure for Direct Numerical Simulation of Turbulence," The J. Sci. Computing, Vol. 38 (11), 1996, pp. 215-242.

[12] Cai, X, Ladeinde, F. & O'Brien, E. E., "Parallel DNS on the SP2 with MPI," *Advances in DNS/LES*. C. Liu & Z. Liu, Eds. Greyden Press, Columbus, 1997, pp. 491-498.

[13] Williams, F.A., "Combustion Theory: Fundamental Theory of Chemically Reacting Flow Systems," Bengam/Cummings Publishing Co., Menlo Park, California, 1985.

[14] Livescu, D., Jaberi, F. A., and Madnia, C. K., "Direct numerical simulation of reacting turbulent shear flows," APS/DFD Meeting Philadelphia, 1998.

Table: The constants in the 25-step reaction system

No.	A_f	B_f	C_f	A_b	B_b	C_b
1	5.0×10^{17}	-1.0	25000	8.0×10^{15}	0	-1000
2	1.1×10^{16}	0	32712	1.1×10^{15}	0	-941
3	5.5×10^{18}	-1.0	51987	1.8×10^{18}	-1.0	0
4	7.2×10^{18}	-1.0	59340	4.0×10^{17}	-1.0	0
5	5.2×10^{21}	-1.5	59386	4.4×10^{20}	-1.5	0
6	8.5×10^{18}	-1.0	50830	7.1×10^{18}	-1.0	0
7	1.7×10^{16}	0	23100	1.1×10^{16}	0	-440
8	5.8×10^{13}	0	9059	5.3×10^{12}	0	503
9	8.4×10^{13}	0	10116	2.0×10^{13}	0	2600
10	2.2×10^{14}	0	8455	1.5×10^{13}	0	0
11	7.5×10^{13}	0	5586	3.0×10^{13}	0	4429
12	1.7×10^{13}	0	24232	5.7×10^{11}	0	14922
13	1.9×10^{13}	0	24100	1.3×10^{13}	0	0
14	1.7×10^{11}	0.5	21137	6.0×10^{13}	0	0
15	5.8×10^{11}	0.5	28686	3.0×10^{13}	0	0
16	3.7×10^{11}	0.64	27840	1.0×10^{13}	0	0
17	2.0×10^{11}	0.5	36296	1.2×10^{13}	0	0
18	1.2×10^{12}	0.21	39815	1.7×10^{13}	0	12582

19	5.0×10^{13}	0	37940	1.1×10^{13}	0	0
20	1.7×10^{14}	0	24500	4.5×10^{13}	0	0
21	2.4×10^{11}	0.5	19200	1.0×10^{12}	0.5	3120
22	2.0×10^{11}	0.5	15500	3.5×10^{14}	0	740
23	1.0×10^{12}	0	22800	1.0×10^{13}	0	302
24	2.4×10^{13}	0	14500	5.0×10^{11}	0.5	1500
25	1.0×10^{11}	0.5	6000	3.0×10^{12}	0.5	1200